Biomedical Signal Processing and Control 63 (2021) 102229

Contents lists available at ScienceDirect

Biomedical Signal Processing and Control

journal homepage: www.elsevier.com/locate/bspc

An EEG-based methodology for the estimation of functional brain connectivity networks: Application to the analysis of newborn EEG seizure

Ali Kareem Abbas [a], Ghasem Azemi [a,*], Samin Ravanshadi [a], Amir Omidvarnia [b,c]

[a] Faculty of Electrical and Computer Engineering, Razi University, Kermanshah, Iran
[b] Institute of Bioengineering, Swiss Federal Institute of Technology (EPFL), Campus Biotech, Chemin des Mines 10, 1202, Geneva, Switzerland
[c] Department of Radiology and Medical Informatics, CIBM, University of Geneva, Geneva, Switzerland

ARTICLE INFO

Keywords:
EEG
Brain connectivity analysis
Newborn seizure
Phase synchrony
Graph measures

ABSTRACT

This study presents a new methodology for obtaining functional brain networks (FBNs) using multichannel scalp EEG recordings. The developed methodology extracts pair-wise phase synchrony between EEG electrodes to obtain FBNs at δ, θ, and α -bands and investigates their network properties in presence of seizure to detect multiple facets of functional integration and segregation in brain networks. Statistical analysis of the frequency-specific graph measures during seizure and non-seizure intervals reveals their highly discriminative ability between the two EEG states. It is also verified by performing the receiver operating characteristic (ROC) analysis. The results suggest that, for the majority of subjects, the FBNs during seizure intervals exhibit higher modularity and lower global efficiency compared to the FBNs during non-seizure intervals; meaning that during seizure activities the networks become more segregated and less aggregated. Some differences in the results obtained for different subjects can be attributed to the subject-specific nature of seizure networks and the type of epileptic seizure the subject has experienced. The results demonstrate the capacity of the proposed framework for studying different abnormal patterns in multichannel EEG signals.

1. Introduction

Brain connectivity analysis aims at describing how different regions of the brain are connected. There are three types of connectivity: (*i*) structural connectivity which refers to the existence of anatomical links between different brain areas, (*ii*) functional connectivity, and (*iii*) effective connectivity which are estimated by measuring statistical dependencies and causal interaction between time-series of different brain regions, respectively [1]. Brain connectivity has been well studied using different neuroimaging techniques such as electroencephalography (EEG), magnetoencephalography (MEG), computed tomography (CT), functional magnetic resonance imaging (fMRI), functional near-infrared spectroscopy (fNIRS), and positron emission tomography (PET) [2–7]. Such neuroimaging techniques have been used to study brain function in health as well as neurological disorders including epilepsy, autism, and schizophrenia [3,8]. The recent trend has been towards using multimodal measurements to obtain complementary data on neural communication, with the aim to get a more comprehensive understanding of functional brain dynamics [9,10]. Several neuroimaging studies have used connectivity analysis methods to extract clinical information about the topology and dynamics of abnormal functional brain networks (FBNs) [5,11–16]. For example, in [17], simultaneously acquired EEG and fMRI data were used to make informed inferences about observed functional network connectivity dynamics and demonstrated that estimated dynamic functional network connectivity states correspond to distinct electrophysiological mental states. However, the results may still be significantly influenced by the way that FBNs are constructed from the neuroimaging datasets and the choice of graph metrics which are extracted from the networks [18–20].

Amongst different neuroimaging tools, EEG is widely used for studying the dynamics of brain function due to its high temporal resolution which makes it useful for tracking and analysis of cortical electrical activity [21]. In particular, scalp-level EEG is a non-invasive recording and relatively low cost modality which is widely used for characterization of dynamical behavior in FBNs for classification of different EEG states, analysis of variance [22], logistic regression, support vector machine and Naïve Bayesian [23], graph convolutional neural network (GCNN) [24]. Most commonly used signal connectivity measures for multichannel EEG analysis include: phase synchrony (PS) [25,26], magnitude squared coherence [27], phase lag index (PLI) [28,

* Corresponding author.
E-mail address: g.azemi@razi.ac.ir (G. Azemi).

https://doi.org/10.1016/j.bspc.2020.102229
Received 18 June 2020; Received in revised form 28 August 2020; Accepted 18 September 2020
Available online 28 September 2020
1746-8094/© 2020 Elsevier Ltd. All rights reserved.

29], and amplitude envelope correlation [30]. In [29], the PLI is used to construct the static network of each EEG sliding window and, by sorting the static network according to the time series, to construct the temporal brain networks. The study uses the temporal brain networks to investigate the dynamic functional connectivity of the human brain in different emotional EEG states, taking into account the time-varying regional brain activity. The main drawback of such techniques, however, is the effect of volume conduction on multichannel EEG scalp-level signals, which may produce spurious and distorted connectivity results from focal brain activity [31–33]. In order to overcome the volume conduction problem, some studies, e.g. [6], have applied source localization techniques to scalp EEG signals for studying FBNs when subject is performing a task. The influence of the volume conduction on various functional connectivity metrics is studied in [32] by integrating a surface-based computational model of the human head and a model of coupled oscillators simulating the electrical activity of brain sources.

In this paper, a new methodology for studying functional brain connectivity is presented and applied to multichannel newborn EEG signals to reveal cortical networks during seizure and non-seizure EEG periods. The proposed methodology is based on measuring statistical coupling between different EEG channels through the degree of phase synchrony between them using the circular omega complexity (COC) measure [34]. We have already shown that the COC measure is relatively insensitive to volume conduction in the analysis of scalp multichannel EEG signals. The resulted connectivity matrices are then used to generate a graph-based representation of FBNs. The FBNs are analyzed using selected graph features with the aim of identifying differences in brain networks during seizure and non-seizure states. In this study, we examine three hypotheses associated with newborn EEG signals in the presence of abnormality: (*i*) connectivity patterns of newborn EEG-based FBNs are significantly affected by seizure, (*ii*) these changes in functional brain connectivity can be detected by measuring phase synchrony between scalp EEG electrodes, and (*iii*) FBNs become more modular and less efficient during seizure intervals. In this context, *modularity* is defined as the degree to which the network can be subdivided into non-overlapping groups or modules of nodes and *global efficiency* is described as the average inverse shortest path length in the network [35]. To evaluate the three hypotheses, we design an analysis framework based on our previously developed measure of signal connectivity, i.e., COC measure, and apply it on a database of 14 newborn EEG datasets with seizure and non-seizure states [36].

The rest of the paper is organized as follows: Section 2 describes the multichannel newborn EEG database used in this study and introduces the proposed methodology for estimating brain networks using multichannel scalp EEG signals. In Section 3, the experimental results of applying the proposed methodology to the newborn EEG database are presented and discussed. The paper is concluded in Section 4.

2. Materials and methods

2.1. The EEG database

This study uses a recently released database composed of multichannel EEG signals collected at the Helsinki University Hospital from 79 infants (either before 35 or after 45 weeks post-menstrual age) admitted to the neonatal intensive care unit. The signals were recorded at the sampling rate of 256 Hz using the NicOne EEG amplifier with 19 electrodes positioned and referenced to the right or left earlobes according to the 10–20 international system of electrode placement. Among the 79 EEG datasets in the database, 39 datasets composed of both seizure and non-seizure intervals. Seizure and non-seizure epochs in all the multichannel datasets were labeled by 3 experts. More details about this neonatal EEG database can be found in [36].

2.2. Extraction of FBNs from multichannel newborn EEG

The adapted methodology for the estimation of FBN using multichannel EEG signals consists of four main steps as shown in Fig. 1. The steps are described in the following sections.

2.2.1. Pre-processing

EEG signals are usually contaminated by various physiological and non-physiological sources of activity. Removing these artifacts is a crucial step for producing noise-free signals suitable for brain connectivity analysis. This study used stationary wavelet transform to enhance the EEG datasets under-analysis. The signals were then visually inspected and remaining artifacts were removed manually. After this pre-processing, EEG datasets with seizure activities of more than 5 min length were selected; resulted in 14 datasets with details given in Table 1.

In this study, 150 seizure and 150 non-seizure epochs of length 3 s with 1 s overlaps were extracted from EEG signals of each subject. The length of EEG epochs was chosen based on previous studies in this field, e.g. [36]. Finally, 3 band-pass filters were deployed to decompose EEG epochs into 3 commonly-used EEG frequency bands, i.e. δ -band (0.5−4 Hz), θ -band (4−8 Hz), and α -bnad (8−13 Hz). This is based on the reports by previous studies suggesting that seizures have spectral activities mostly below 12 Hz [37,38].

2.2.2. Estimation of FBNs

This study, we applied the multivariate PS measure introduced in [34], i.e. the COC measure, to the pre-processed multichannel EEG signals for construction of the connectivity matrices (CMs). This measure is briefly introduced in the following section. We chose the COC measure because: (*i*) it is relatively insensitive to volume conduction and (*ii*) it has been shown to have better performance in identifying PS in multivariate signals such as multichannel EEG in contrast to other PS measures [34].

2.2.2.1. The circular omega complexity (COC) measure. In order to measure the PS between two signals, their instantaneous phases (IPs) need to be estimated first. For mono-component signals with a single ridge in the time-frequency domain, this can be achieved by using the Hilbert transform. In this approach, the IP of a real discrete signal $x[n]$, i.e. $\varphi_x[n]$, is estimated as:

$$\varphi_x[n] = \tan^{-1}\left(\frac{\widehat{x}[n]}{x[n]}\right) \tag{1}$$

where $\widehat{x}[n]$ is the Hilbert transform of the signal $x[n]$. Using the COC measure, the PS between 2 mono-component signals $x_k[n]$ and $x_l[n]$ with corresponding IPs, $\phi_k[n]$ and $\phi_l[n]$, $n = 0, 1, \ldots, N-1$, is estimated as:

$$\eta_{k,l} = \frac{\sum_{n=0}^{N-1} \sin(\phi_k[n] - \overline{\phi}_k)\sin(\phi_l[n] - \overline{\phi}_l)}{\sqrt{\sum_{n=0}^{N-1} \sin^2\phi_k[n] - \overline{\phi}_k)\sin^2(\phi_l[n] - \overline{\phi}_l)}} \tag{2}$$

where $\overline{\phi}_k$ is the circular mean of $\phi_k[n]$ given by:

$$\overline{\phi}_k = \arg\left(\sum_{n=0}^{N-1} e^{i\phi_k[n]}\right) \tag{3}$$

The COC measure $\eta_{k,l}$ takes values between 0 and 1; where the value of 0 indicates no PS between the two signals. Using the pair-wise PS values found using (2) for all EEG electrodes, a matrix is formed as:

$$\boldsymbol{\eta} = \left[\eta_{k,l}\right]_{C\times C} \tag{4}$$

where C is the number of EEG electrodes. As mentioned earlier in Section 2.2.1, the multichannel EEG epoch under-analysis is decomposed in

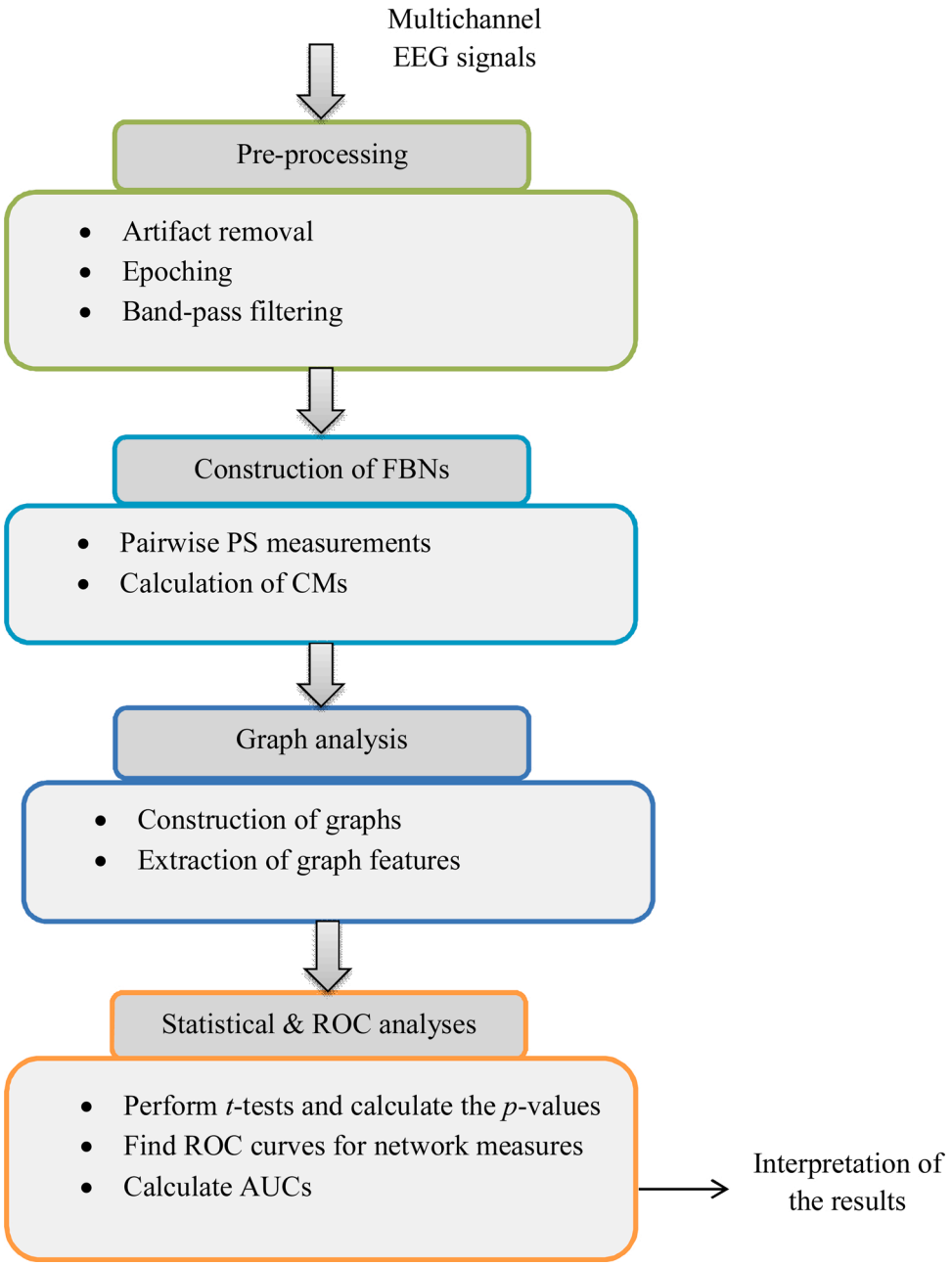

Fig. 1. Block diagram of the adapted methodology for the estimation of FBNs from newborn seizure signals. Abbreviations: PS: phase synchrony, CM: connectivity matrix, ROC: receiver operating characteristic and AUC: area under the ROC curve.

to 3 frequency bands, δ, θ, and α -bands, at the pre-processing stage. This is to satisfy the Bedrosian requirement for the instantaneous phase signals, namely the narrow-band condition for the input signals. The COC matrix corresponding to each frequency band is found using (2)–(4). These 3 matrices $\boldsymbol{\eta}^{(\delta)}$, $\boldsymbol{\eta}^{(\theta)}$ and $\boldsymbol{\eta}^{(\alpha)}$ are used as CMs to construct undirected weighted graphs characterizing the FBNs during seizure and non-seizure activities as explained in the next section.

2.2.2.2. Graph properties of FBNs. Functional brain networks can be modelled as *graphs* whose *edges* are associated with the connectivity strength between *brain nodes* [35]. In the current study, the graph nodes represent locations of the EEG electrodes and edges are associated with the COC values between EEG electrodes.

2.2.3. Graph analysis

In order to quantitatively compare the resulted FBNs for seizure and non-seizure epochs, graph measures can be extracted from the visualized FBNs obtained in Section 2.2.2.2. In this study, six graph measures were chosen to detect multiple facets of functional integration and segregation in brain networks and characterize one or more aspects of global and local brain connectivity. The measures are briefly introduced below; more details about them and their formulas can be found in [35,39–42].

1 The ***Global efficiency*** (GE) of a given network is defined as the average inverse shortest path length in the network and is inversely related to the characteristic path length, i.e. the average shortest path length for all pairs of nodes. In networks with high global efficiency the information is exchanged across the whole network more efficiently.

Table 1
Details about the EEG seizure and non-seizure epochs used in this study. Subject IDs are according to the indexing of [36].

Subject ID	Length of the pre-processed recording (in sec)	seizure length (in sec)	non-seizure length (in sec)
4	3426	850	2127
5	3842	3136	492
9	3551	862	2507
13	15,417	1235	13,980
14	3727	2084	1221
19	9007	2089	6311
38	6096	2681	1576
39	4630	2177	2065
44	3361	315	2961
52	3921	86	3790
66	11,351	1548	9470
67	4901	1342	3097
75	3956	918	3030
78	4972	1915	2341

2 The ***modularity*** (M) quantifies the degree to which the network can be subdivided into non-overlapping groups or modules of nodes. Networks with dense connections between the nodes within groups but sparse connections between nodes in different modules exhibit high modularity.
3 The ***mean weighted clustering coefficient*** (MWCC) over all the nodes in a graph measures the degree to which the nodes in the network tend to cluster together. Networks having more nodes completely associated with each node exhibit high mean weighted clustering coefficient.
4 The ***mean closeness centrality*** (MCC) of a network indicates how the nodes are close to each other and therefore depends on the length of the routes from one node to other nodes. In networks with high mean closeness centrality, the nodes are closer to each other.
5 ***Clustering coefficient entropy*** (CCE) measures the distribution of the clustering coefficient of the nodes in a network using Shannon's entropy of nodes' clustering coefficients. It characterizes the inherent structure of the network in a way that its value for networks with only few nodes with complete neighborhood is low.
6 The ***average degree*** (AD) shows the average number of edges per node in a network. In networks with more connections, the average degree is higher.

2.2.4. Statistical and ROC analyses

In order to validate the proposed approach for visualizing the FBNs using multichannel EEG signals, the obtained networks during seizure and non-seizure states are compared statistically and quantitatively. This is achieved by first extracting the six graph measures introduced in Section 2.2.3 from the graphs representing the FBNs during seizure and non-seizure states. Then the *t*-test is performed on the values of each feature for all the seizure and non-seizure epochs and the *p*-values are used to check the statistical difference between the values of that measure for seizure and non-seizure states. The ability of each network measure in discriminating between the two classes is also quantitatively measured by performing the receiver operating characteristics (ROC) analysis [43]. For a given network measure, the ROC curve plots the sensitivity of a binary classifier which uses that measure to classify the two groups, as a function of 1-(its specificity), as its discrimination threshold is varied. The area under the resulting ROC, i.e. AUC, for each measure is calculated and used as an explanation of the ROC curve. The AUC values range from 0.5 to 1 where 1 represents the optimal classifier and the value of 0.5 refers to a random guessing classifier.

3. Results

The results of applying the proposed method to the multichannel EEG datasets detailed in Table 1 are presented in this section. The main algorithm was implemented in MATLAB and the functional brain graphs were visualized using the BrainNet Viewer toolbox [44] based on the computed CMs. The graph measures presented in Section 2.2.3 were extracted using the Brain-connectivity toolbox [35].

3.1. FBNs during seizure and non-seizure states

For each subject, the adapted methodology explained in Section 2.2 was applied to 150 seizure and 150 non-seizure 19-channel EEG epochs of length 3 s with 1 s overlaps. Once the CMs were calculated in δ, θ, and α -bands using the COC measure, the FBNs in each frequency band were visualized using graphs with nodes located at the position of EEG electrodes. In this way, the existence of operating functional sub-networks in the brain is expressed by the color-coded links of a graph. The graphs identify different brain regions that are generally synchronized and indicate the presence and strength of functional connectivity between each two cortical regions, as represented by the two corresponding electrodes, in the current brain state.

Fig. 2 illustrates the resulted graphs visualizing the FBNs during non-seizure states for Subject 9, as an exemplary subject, with color-coded links showing the strength of the connection between each two electrodes. A threshold value of 0.3 was used to show links with significant strength, i.e. only links are shown for which the strength is more than 30 % of the maximum strength in the graph. Similar procedures were used to obtain FBNs during seizure states for Subject 9 which are depicted in Fig. 3. The corresponding CMs for Subject 9 are shown in Figs. 4 and 5.

3.2. Statistical and ROC analyses of FBNs

The networks obtained during seizure and non-seizure states were statistically and quantitatively compared based on the extracted graph measures. First the 6 graph measures introduced in Section 2.2.5 were extracted from the CMs used to build the FBNs. Then the *t*-test was performed on the values of each network measure for all the seizure and non-seizure epochs in the 3 bands for each subject and the *p*-values were found. The results are reported in Table 2.

The ROC analysis was also performed and the AUC for each network measure was calculated. Table 2 shows the AUC values for each network measure in each of the three frequency bands for each subject. And for illustration, box plots of all the features for Subject 9 are depicted in Fig. 6, showing how their values are spread out for seizure and non-seizure epochs in the 3 bands.

4. Discussion

The findings of this study are three-fold: (*i*) the results suggest that the topological structure and connectivity patterns across FBNs extracted from newborn EEG significantly change in the presence of seizure, (*ii*) the COC measure can highlight these changes of functional connectivity in brain networks over different EEG frequency bands and (*iii*) COC-based FBNs present higher modularity and lower global efficiency during ictal states in contrast to interictal states. However, some variations were observed in the results over subjects which can be related to differences in the location of the epileptogenic zones and seizure type across patients. An advantage of PS measures such as COC for EEG-based functional connectivity studies is that they are insensitive to amplitude changes, an important factor which can be easily affected by different types of artifacts. We showed that the adapted framework of this study can be effectively used to discriminate between seizure and non-seizure EEG states with high accuracy. It reinforces that the definition of functional brain connectivity based on the level of global phase synchrony across EEG electrodes could be an efficient way for the development of discriminative features between seizure and non-seizure intervals in multichannel newborn EEG recordings. These findings add to the results of previous neuroimaging studies reporting functional connectivity changes in the presence of neonatal seizure and may be used for the

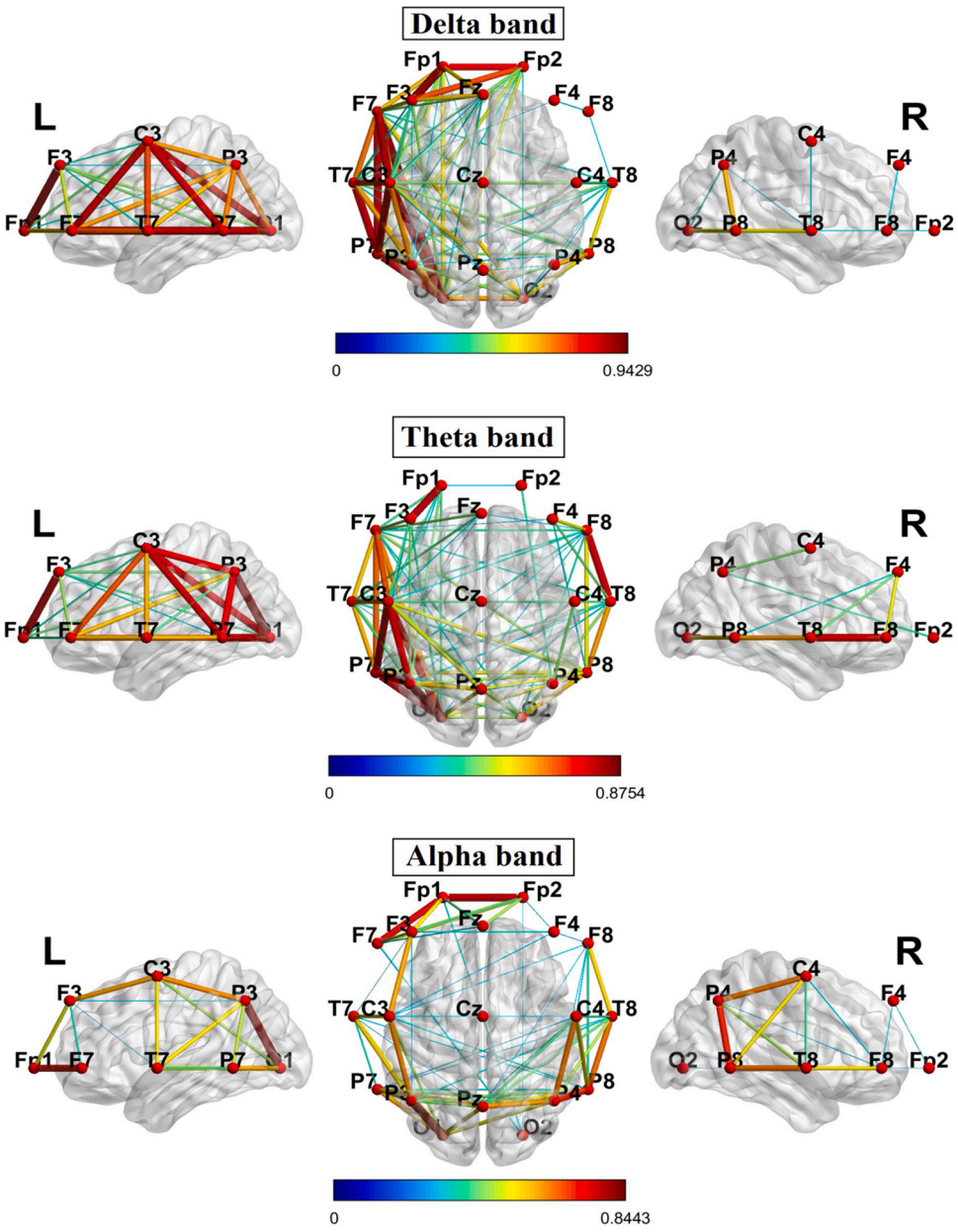

Fig. 2. Weighted functional brain connectivity networks for Subject 9 during non-seizure states for δ, θ, and α -bands with threshold value of 0.3.

development of newborn seizure detection/prediction systems.

As illustrated in Figs. 2 and 3, the proposed approach provides FBNs during different brain states from multichannel scalp EEG signals. Characterization of phase-based FBNs in the presence of seizure is challenging due to the difference in the location of seizure onset zones over subjects. In other words, seizure foci could be localized in space or generalized over multiple electrodes. This and also the type of the seizure the subject has experienced lead to significant difference in the temporal and spectral features of seizure and non-seizure periods in subjects. Generalized phase synchrony measures such as COC are well suited to this purpose, because they can consider a comprehensive picture of the global disruption across multiple EEG electrodes regardless of the source of the seizure event in time and space. Given the subject-specific nature of seizure networks in the newborn EEG datasets of this study, we chose to report the results in a case-by-case basis. The methodology used in this research has the capacity to be used to identify neural networks involved in normal and pathological brain function and can therefore aid clinicians in the diagnosis and estimation of neurodevelopmental disorders.

As shown in the exemplary Figs. 2 and 3 as an example, the spatial topology of FBNs suggest that the majority of strong connections in non-seizure states tend to be between neighboring electrodes, in particular, across prefrontal areas (Fp1 and Fp2). It extends towards the left hemisphere locations as shown in the graphs associated with the δ and θ frequency bands in Fig. 2. While the strong connections between near sources were depicted in α. On the other hand, connections also reach faraway regions in seizure states. 30 % of connections are between frontal and occipital lobes. Some differences during seizure sates can also be observed in 3 bands of visualizing brain networks. Subject 9 graphs show strong connectivity compacted between nearby sources (as shown in Fig. 3), whereas frontal pole electrodes reach both posterior and occipital electrodes (as shown in Fig. 2).

Most of the p-values reported in Table 2 are significant (less than 0.05) in almost all EEG frequency bands. It suggests that frequency-specific graph features of the COC-based connectivity matrices extracted from multichannel newborn EEG signals are highly discriminative

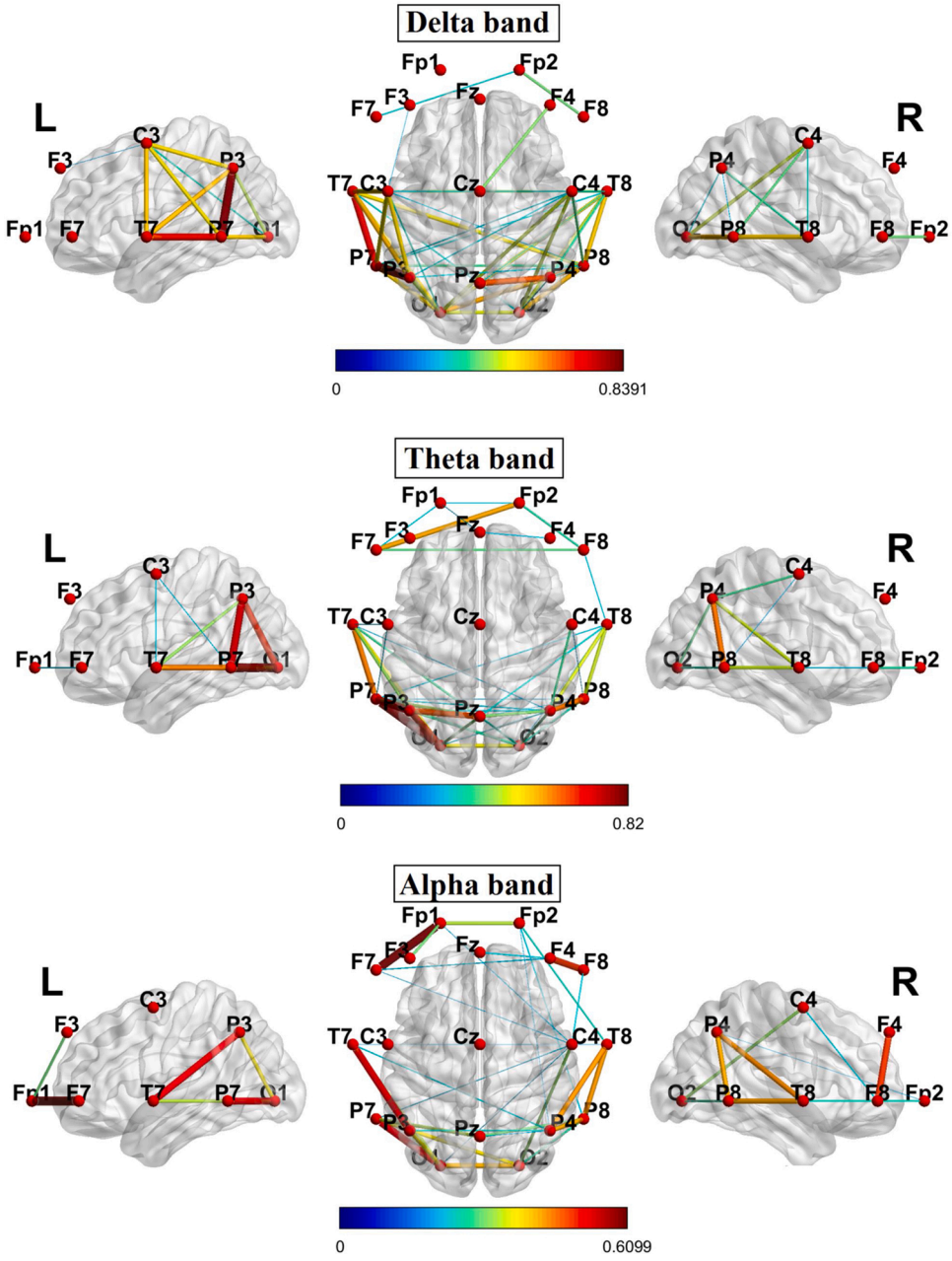

Fig. 3. Weighted functional brain connectivity networks for Subject 9 during seizure states for δ, θ, and α -bands with threshold value of 0.3.

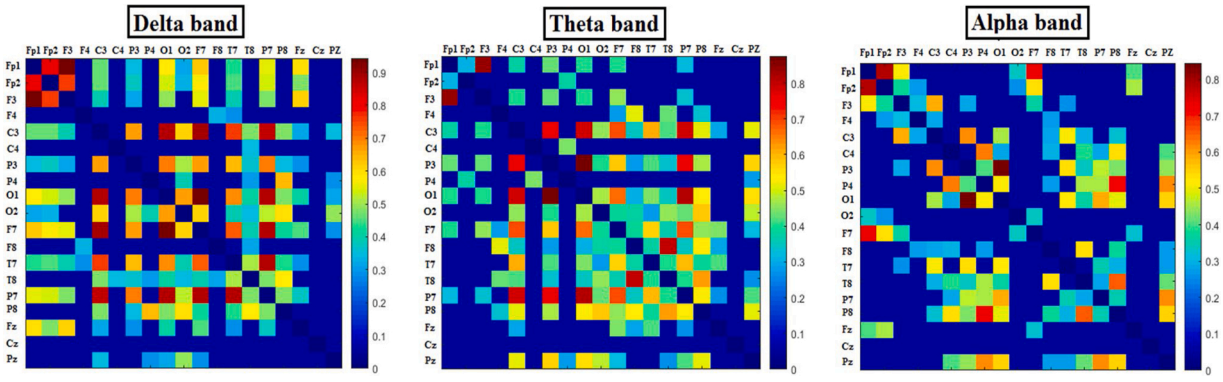

Fig. 4. Connectivity matrices representing FBNs in δ, θ, and α -bands for Subject 9 during non-seizure states.

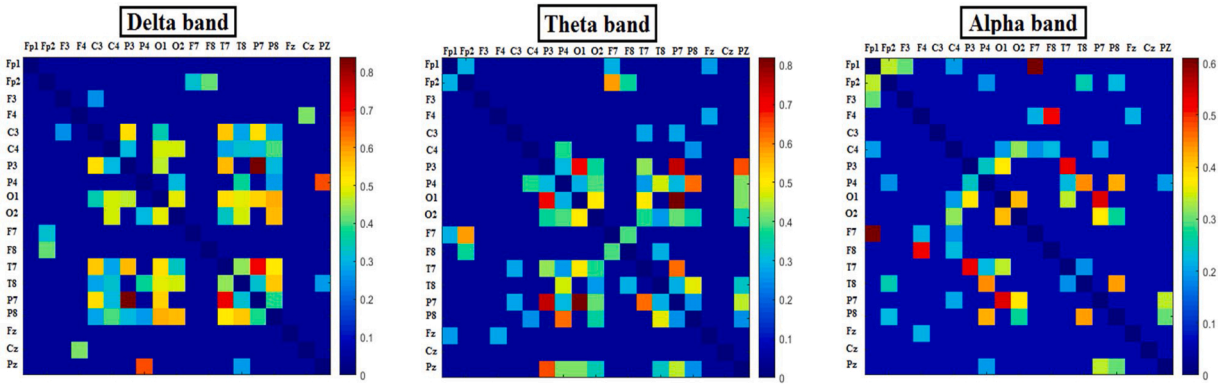

Fig. 5. Connectivity matrices representing FBNs in δ, θ, and α -bands for Subject 9 during seizure states.

Table 2
Results of statistical and ROC analyses of the 6 selected graph measures in different frequency bands for each subject. The p-values (*: $p < 0.05$;**: $p < 0.001$) and AUC values (in parentheses) are reported. Acronyms are as follows: GE: Global Efficiency, M: Modularity, MWCC: Mean Weighted Clustering Coefficient, MCC: Mean Clustering Coefficient, CCE: Closedness Centrality Entropy, AD: Average Degree.

Subject ID	Frequency band	Graph measures					
		GE	M	MWCC	MCC	CCE	AD
	Delta	(0.5200)	(0.5531)	(0.5071)	(0.5300)	* (0.6010)	(0.5272)
04	Theta	** (0.7811)	** (0.6311)	** (0.7613)	** (0.6628)	* (0.6074)	** (0.7879)
	Alpha	** (0.9461)	** (0.6832)	** (0.8621)	** (0.8431)	** (0.6286)	** (0.9406)
	Delta	** (0.6460)	** (0.6333)	** (0.6534)	** (0.6265)	(0.5021)	** (0.6428)
05	Theta	* (0.5670)	** (0.7442)	** (0.6549)	(0.6052)	* (0.5868)	* (0.5926)
	Alpha	(0.5404)	** (0.7847)	** (0.6772)	(0.5850)	* (0.6057)	(0.5041)
	Delta	** (0.7393)	** (0.6924)	** (0.7361)	** (0.6719)	(0.5425)	** (0.7430)
09	Theta	** (0.7510)	** (0.7752)	** (0.7626)	** (0.7356)	* (0.6115)	** (0.7608)
	Alpha	** (0.6666)	* (0.5634)	** (0.6622)	(0.6084)	** (0.6086)	** (0.6684)
	Delta	* (0.5638)	(0.5652)	* (0.5813)	* (0.6305)	* (0.5787)	* (0.5649)
13	Theta	* (0.5710)	** (0.6133)	** (0.6576)	** (0.6412)	(0.5620)	* (0.5890)
	Alpha	** (0.7967)	** (0.7501)	** (0.8169)	** (0.7724)	(0.5472)	** (0.8058)
	Delta	** (0.6704)	** (0.7506)	** (0.7351)	** (0.6997)	(0.5025)	** (0.6931)
14	Theta	** (0.6963)	** (0.7627)	** (0.7760)	** (0.7216)	* (0.5728)	** (0.7216)
	Alpha	** (0.7178)	(0.5116)	** (0.7033)	** (0.6802)	** (0.7291)	** (0.7151)
	Delta	(0.5365)	* (0.5618)	(0.5092)	(0.5002)	(0.5262)	(0.5298)
19	Theta	* (0.5708)	* (0.5770)	(0.5032)	(0.5520)	(0.5490)	* (0.5592)
	Alpha	* (0.6198)	* (0.5802)	* (0.6233)	(0.5333)	* (0.5946)	* (0.6180)
	Delta	** (0.5974)	(0.5491)	(0.5667)	* (0.6181)	(0.5449)	* (0.5901)
38	Theta	** (0.6340)	** (0.6553)	** (0.6653)	(0.5692)	* (0.5754)	** (0.6415)
	Alpha	** (0.7841)	** (0.7624)	** (0.7935)	** (0.7342)	(0.5772)	** (0.7854)
	Delta	(0.5692)	(0.5117)	(0.5783)	** (0.6305)	** (0.6172)	(0.5719)
39	Theta	(0.5719)	* (0.5752)	* (0.6382)	** (0.6734)	** (0.6986)	(0.5866)
	Alpha	* (0.5400)	* (0.5981)	(0.5266)	(0.5444)	(0.5030)	(0.5417)
	Delta	** (0.6786)	(0.5197)	** (0.6125)	(0.5594)	** (0.6993)	** (0.6787)
44	Theta	** (0.7288)	* (0.6003)	** (0.6634)	(0.5935)	(0.5734)	** (0.7180)
	Alpha	(0.5528)	(0.5434)	(0.5021)	(0.5272)	(0.5091)	(0.5450)
	Delta	* (0.6830)	(0.6617)	(0.6714)	* (0.6839)	(0.6410)	* (0.6843)
52	Theta	* (0.8125)	(0.6305)	(0.6796)	(0.6532)	* (0.7282)	* (0.8060)
	Alpha	(0.5795)	* (0.6762)	* (0.7041)	* (0.6178)	(0.5177)	(0.5778)
	Delta	** (0.6208)	(0.5642)	* (0.6042)	(0.5480)	(0.5409)	* (0.6132)
66	Theta	** (0.6787)	* (0.6008)	** (0.6643)	* (0.5649)	(0.5176)	** (0.6713)
	Alpha	** (0.7964)	(0.5557)	** (0.6121)	* (0.6081)	* (0.6247)	** (0.7812)
	Delta	** (0.6220)	(0.5218)	** (0.6026)	* (0.6035)	(0.5157)	** (0.6215)
67	Theta	** (0.6452)	(0.5191)	* (0.5705)	(0.5087)	(0.5329)	** (0.6332)
	Alpha	(0.5356)	** (0.6181)	** (0.6243)	* (0.5849)	* (0.5823)	(0.5053)
	Delta	** (0.6404)	* (0.5772)	** (0.6455)	* (0.6109)	(0.5149)	** (0.6332)
75	Theta	** (0.6888)	* (0.5910)	** (0.7039)	** (0.7307)	** (0.7052)	** (0.6892)
	Alpha	** (0.9948)	** (0.7034)	** (0.9922)	** (0.9989)	** (0.9085)	** (0.9932)
	Delta	** (0.6521)	** (0.6568)	** (0.6425)	* (0.5910)	* (0.5721)	** (0.6489)
78	Theta	** (0.6580)	** (0.7029)	** (0.6960)	** (0.6316)	(0.5078)	** (0.6623)
	Alpha	(0.5231)	(0.5439)	* (0.5935)	(0.5701)	** (0.6256)	(0.5013)

between the seizure and non-seizure states. Box plots of Fig. 6 indicate significantly higher modularity and decreased global efficiency in the COC-based graphs of newborn EEG signals in presence of seizure in contrast to the non-seizure periods. This is in line with the graph properties of fMRI-based FBNs in epilepsy subjects where increased segregation and decreased aggregation over networks has been reported [45]. This observation is robust over all frequency bands and implies the importance of topological changes during the ictal and interictal states of newborn EEG. This has also been reflected in the AUC values reported in Table 2. However, one has to be cautious about drawing a rigorous

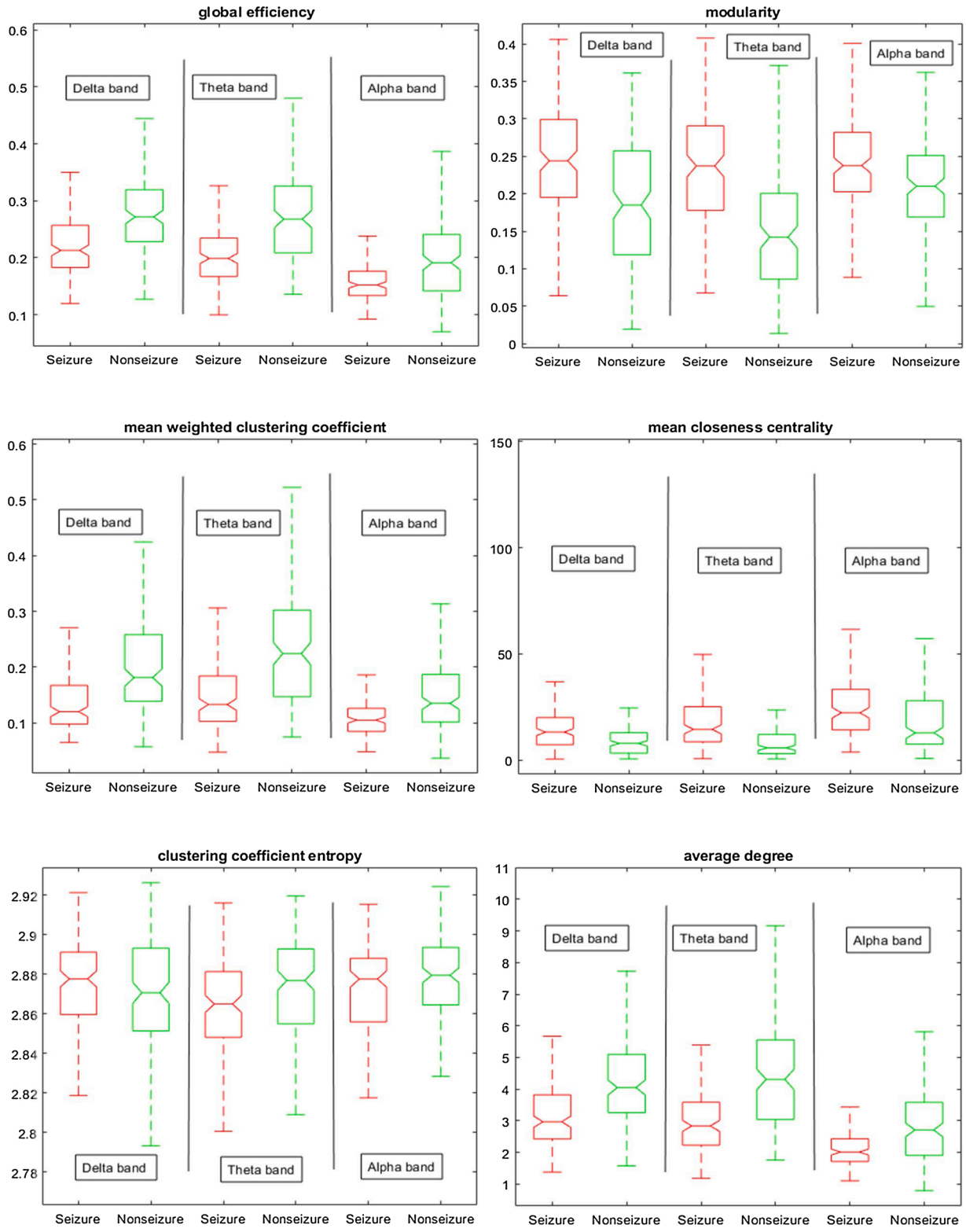

Fig. 6. Box plots of the six selected graph measures in the three frequency bands for Subject 9.

conclusion at this stage due to the small group size and relatively small number of the seizure/non-seizure EEG segments in our study. A large variety of graph measures have been proposed for investigating network features of functional brain interactions [35]. Our choice of graph measures in this study, however, was mainly based on the importance of modularity and efficiency in the functional graphs associated with seizure and non-seizure data. For example, it has been suggested that the nodes in epileptic FBNs extracted from fMRI datasets of focal epilepsy patients become more segregated and less aggregated [45]. In summary, the results of both statistical and ROC analyses for all the subjects follow similar trends and the differences observed in the results can be attributed to the subject-specific nature of seizure networks and the type of epileptic seizure the subject has experienced.

A limitation of this study is associated with its small sample size

which makes it difficult to generalize the findings to large populations. It also remains for future research to repeat it at the EEG source level and investigate the potential differences between the graph measures of scalp phase-based scalp EEG signals with their corresponding source level activity during seizure and non-seizure states.

5. Conclusion

Combined information of newborn EEG-based FBNs in the time, frequency and space (i.e., electrode location) is useful for discrimination of seizure and non-seizure states. The adapted methodology of this study has the capacity to reveal subtle changes in the graph properties of FBNs in the presence of newborn seizures at different EEG frequency bands. It supports the hypothesis that newborn seizure can significantly affect the functional brain connectivity patterns in newborns and change the phase relationships across scalp EEG channels. From this perspective, graph measures of phase-based FBNs can be effectively used for EEG signal classification and newborn seizure detection.

CRediT authorship contribution statement

Ali Kareem Abbas: Methodology, Software, Writing - original draft. **Ghasem Azemi:** Supervision, Methodology, Formal analysis, Writing - review & editing. **Samin Ravanshadi:** Supervision, Methodology. **Amir Omidvarnia:** Methodology, Formal analysis, Writing - review & editing.

Declaration of Competing Interest

The authors report no declarations of interest.

Acknowledgement

GA acknowledges financial support from the Iranian Cognitive Sciences and Technologies Council, Iran, through grants 7104 and 8043. AO acknowledges financial support through the Marie Curie EuroTech postdoctoral fellowship, co-funded by the European Commission under its framework programme Horizon 2020 for the project “Towards better understanding of complex dynamics in functional brain connectivity” (Grant Agreement number 754462). AO thanks Prof. Dimitri Van De Ville at the Medical Image Processing lab, Campus Biotech, EPFL, for his valuable support.

References

[1] K.J. Friston, Functional and effective connectivity: a review, Brain Connect. 1 (1) (2011) 13–36.
[2] K. Sameshima, L.A. Baccala, Methods in Brain Connectivity Inference Through Multivariate Time Series Analysis, CRC press, 2016.
[3] M.C. Stevens, The developmental cognitive neuroscience of functional connectivity, Brain Cogn. 70 (1) (2009) 1–12.
[4] J.G.N. Galán, Functional and Effective Connectivity in MEG. Application to the Study of Epilepsy, Universidad Politécnica de Madrid, 2013.
[5] M. Hassan, F. Wendling, Electroencephalography Source Connectivity: Toward High time/space Resolution Brain Networks, arXiv preprint arXiv:1801.02549, 2018.
[6] M. Hassan, P. Benquet, A. Biraben, C. Berrou, O. Dufor, F. Wendling, Dynamic reorganization of functional brain networks during picture naming, Cortex 73 (2015) 276–288.
[7] R. Shriram, D.M. Sundhararajan, N. Daimiwal, Brain Connectivity Analysis Methods for Better Understanding of Coupling, arXiv preprint arXiv:1212.3786, 2012.
[8] O. David, D. Cosmelli, D. Hasboun, L. Garnero, A multitrial analysis for revealing significant corticocortical networks in magnetoencephalography and electroencephalography, Neuroimage 20 (1) (2003) 186–201.
[9] P. Bright, Neuroimaging: Methods, BoD–Books on Demand, 2012.
[10] A. Tokariev, Studying connectivity in the neonatal EEG. Dissertationes Scholae Doctoralis Ad Sanitatem Investigandam Universitatis Helsinkiensis, 2015.
[11] M. Hassan, O. Dufor, I. Merlet, C. Berrou, F. Wendling, EEG source connectivity analysis: from dense array recordings to brain networks, PLoS One 9 (8) (2014) e105041.
[12] X. Wu, W.-L. Zheng, B.-L. Lu, Identifying functional brain connectivity patterns for EEG-based emotion recognition, in: 2019 9th International IEEE/EMBS Conference on Neural Engineering (NER), IEEE, 2019, pp. 235–238.
[13] C.M. Tyng, H.U. Amin, N.M. Saad, M. Abdul Rahman, A.S. Malik, T.B. Tang, Exploring EEG effective connectivity network in estimating influence of color on emotion and memory, Front. Neuroinform. 13 (2019) 66.
[14] P. van Mierlo, Y. Höller, N.K. Focke, S. Vulliemoz, Network perspectives on epilepsy using EEG/MEG source connectivity, Frontiers Neurol. Rev. 10 (721) (2019) (in English),July-17 2019.
[15] A. Kabbara, H. Eid, W. El Falou, M. Khalil, F. Wendling, M. Hassan, Reduced integration and improved segregation of functional brain networks in Alzheimer’s disease, J. Neural Eng. 15 (2) (2018) 026023.
[16] E. Olejarczyk, W. Jernajczyk, Graph-based analysis of brain connectivity in schizophrenia, PLoS One 12 (11) (2017) e0188629.
[17] E. Allen, E. Damaraju, T. Eichele, L. Wu, V.D. Calhoun, EEG signatures of dynamic functional network connectivity states, Brain Topogr. 31 (1) (2018) 101–116.
[18] W.H. Lee, S. Frangou, Linking functional connectivity and dynamic properties of resting-state networks, Sci. Rep. 7 (1) (2017) 1–10.
[19] F. Mohagheghian, et al., Computer-aided tinnitus detection based on brain network analysis of EEG functional connectivity, J. Biomed. Phys. Eng. 9 (6) (2019) 687.
[20] E. Paraskevopoulos, N. Chalas, P. Bamidis, Functional connectivity of the cortical network supporting statistical learning in musicians and non-musicians: an MEG study, Sci. Rep. 7 (1) (2017) 1–10.
[21] P. Nunez, E. Harth, Electric fields of the brain: the neurophysics of EEG, PhT 35 (6) (1982) 59.
[22] S. Lagarde, et al., Interictal stereotactic-EEG functional connectivity in refractory focal epilepsies, Brain 141 (10) (2018) 2966–2980.
[23] W. Mumtaz, S.S.A. Ali, M.A.M. Yasin, A.S. Malik, A machine learning framework involving EEG-based functional connectivity to diagnose major depressive disorder (MDD), Med. Biol. Eng. Comput. 56 (2) (2018) 233–246.
[24] M. Wang, H. El-Fiqi, J. Hu, H.A. Abbass, Convolutional neural networks using dynamic functional connectivity for EEG-based person identification in diverse human states, Ieee Trans. Inf. Forensics Secur. 14 (12) (2019) 3259–3272.
[25] J.P. Lachaux, E. Rodriguez, J. Martinerie, F.J. Varela, Measuring phase synchrony in brain signals, Hum. Brain Mapp. 8 (4) (1999) 194–208.
[26] T. Peng, A.B. Rowley, P.N. Ainslie, M.J. Poulin, S.J. Payne, Wavelet phase synchronization analysis of cerebral blood flow autoregulation, IEEE Trans. Biomed. Eng. 57 (4) (2010) 960–968.
[27] J.S. Bendat, A.G. Piersol, Engineering Applications of Correlation and Spectral Analysis, Wiley-Interscience, New York, 1980, p. 315, 1980.
[28] C.J. Stam, G. Nolte, A. Daffertshofer, Phase lag index: assessment of functional connectivity from multi channel EEG and MEG with diminished bias from common sources, Hum. Brain Mapp. 28 (11) (2007) 1178–1193.
[29] X. Liu, et al., Emotion recognition and dynamic functional connectivity analysis based on eeg, IEEE Access 7 (2019) 143293–143302.
[30] M.J. Brookes, M.W. Woolrich, G.R. Barnes, Measuring functional connectivity in MEG: a multivariate approach insensitive to linear source leakage, Neuroimage 63 (2) (2012) 910–920.
[31] J.M. Schoffelen, J. Gross, Source connectivity analysis with MEG and EEG, Hum. Brain Mapp. 30 (6) (2009) 1857–1865.
[32] S.J. Ruiz-Gómez, R. Hornero, J. Poza, A. Maturana-Candelas, N. Pinto, C. Gómez, Computational modeling of the effects of EEG volume conduction on functional connectivity metrics. Application to Alzheimer’s disease continuum, J. Neural Eng. 16 (6) (2019) 066019.
[33] M. Lai, M. Demuru, A. Hillebrand, M. Fraschini, A comparison between scalp-and source-reconstructed EEG networks, Sci. Rep. 8 (1) (2018) 1–8.
[34] P.S. Baboukani, G. Azemi, B. Boashash, P. Colditz, A. Omidvarnia, A novel multivariate phase synchrony measure: application to multichannel newborn EEG analysis, Digit. Signal Process. 84 (2019) 59–68.
[35] M. Rubinov, O. Sporns, Complex network measures of brain connectivity: uses and interpretations, Neuroimage 52 (3) (2010) 1059–1069.
[36] N. Stevenson, K. Tapani, L. Lauronen, S. Vanhatalo, A dataset of neonatal EEG recordings with seizure annotations, Sci. Data 6 (2019) 190039.
[37] A. Temko, W. Marnane, G. Boylan, G. Lightbody, Clinical implementation of a neonatal seizure detection algorithm, Decis. Support Syst. 70 (2015) 86–96.
[38] R.A. Shellhaas, R.R. Clancy, Characterization of neonatal seizures by conventional EEG and single-channel EEG, Clin. Neurophysiol. 118 (10) (2007) 2156–2161.
[39] V. Latora, M. Marchiori, Efficient behavior of small-world networks, Phys. Rev. Lett. 87 (19) (2001) 198701.
[40] M.E. Newman, Fast algorithm for detecting community structure in networks, Phys. Rev. E 69 (6) (2004) 066133.
[41] D. Watts, S. Strogatz, Collective dynamics of “small-world” networks, Nature 393 (1998) 440–442. *View Article*.
[42] Z. Yin, J. Li, Y. Zhang, A. Ren, K.M. Von Meneen, L. Huang, Functional brain network analysis of schizophrenic patients with positive and negative syndrome based on mutual information of EEG time series, Biomed. Signal Process. Control 31 (2017) 331–338.
[43] T. Fawcett, Introduction to receiver operator curves, Pattern Recognit. Lett. 27 (2006) 861–874.
[44] M. Xia, J. Wang, Y. He, BrainNet Viewer: a network visualization tool for human brain connectomics, PLoS One 8 (7) (2013).
[45] M. Pedersen, A. Omidvarnia, J.M. Walz, G.D. Jackson, Increased segregation of brain networks in focal epilepsy: an fMRI graph theory finding, Neuroimage Clin. 8 (2015) 536–542.